



ASIA TURBOMACHINERY & PUMP SYMPOSIUM

23-26 FEBRUARY 2021

SHORT COURSES: 22 FEBRUARY 2021

**ON THE EXPERIMENTAL STATIC AND DYNAMIC LOAD PERFORMANCE OF  
A WATER LUBRICATED HYBRID THRUST BEARING**

**Luis San Andrés**

Mast-Childs Chair Professor  
TEES Turbomachinery Laboratory  
J. Mike Walker '66 Department of  
Mechanical Engineering  
Texas A&M University  
College Station, TX 77845  
[Lsanandres@tamu.edu](mailto:Lsanandres@tamu.edu)

**Scott Wilkinson**

Senior Systems Engineer  
Energy Recovery Inc.  
Houston, TX 77024  
[swilkinson@energyrecovery.com](mailto:swilkinson@energyrecovery.com)

**Jing Yang**

Assistant Research Engineer  
TEES Turbomachinery Laboratory  
J. Mike Walker '66 Department of  
Mechanical Engineering  
Texas A&M University  
College Station, TX 77845  
[yangjing@tamu.edu](mailto:yangjing@tamu.edu)



*Luis San Andrés performs research in lubrication and rotordynamics, having produced advanced technologies of hydrostatic bearings for primary power cryogenic turbo pumps, squeeze film dampers for aircraft jet engines, and gas foil bearings for oil-free micro turbomachinery. Luis is a Fellow of ASME and STLE, and a member of the Industrial Advisory Committees for the Texas A&M Turbomachinery Symposia. Dr. San Andrés has educated dozens of graduate students serving the profession. Dr. San Andrés earned a MS in ME from the University of Pittsburgh and a PhD in ME from Texas A&M University. Luis has published over 250 peer reviewed papers in numerous ASME journals and conferences, including TPS and ATPS. Several papers are recognized as best in various international conferences.*



*Scott Wilkinson received his B.S. and M.S. degrees in Aerospace and Mechanical Engineering, respectively, from Texas A&M University in College Station, TX. As a graduate student, he worked as a research assistant in the Turbomachinery Laboratory under the guidance of Dr. San Andrés. His research focused mainly the experimental analysis of water lubricated thrust bearings including static performance and identification of force coefficients. Scott currently works for Energy Recovery Inc. in Houston, TX as a Senior Systems Engineer.*



*Jing Yang received her B.S. in Thermal and Power Engineering from Huazhong University of Science and Technology, China in 2010 and Ph.D. degree in Fluid Mechanics from Peking University, China in 2017. After graduation, she worked for three years as a post-doctoral Research Associate at the TEES Turbomachinery Laboratory. Since October 2019 Jing continues at the Turbo Lab as an Assistant Research Engineer. Jing Yang's research mainly focuses on the numerical prediction (computational fluid dynamics and bulk flow model) and experimental verification of the dynamic forced performance of annular pressure seals and fluid film bearings.*

**ABSTRACT**

Fluid film thrust bearings (TBs) carry axial loads and control the position of rotating machinery thus enabling tight clearances for the efficient aerodynamic operation of impellers in pumps and compressors. Prediction of thrust forces is largely empirical, emphasizing the need to test TBs for use in reliable rotating machinery equipment. This paper presents a water lubricated test rig housing a pair of hydrostatic TBs and describes the experimental quantification of their static and dynamic forced performance. The test rig comprises of a drive motor, a coupling and quill shaft, and a rigid rotor with two end collars facing the TB elements. Water lubricated radial bearings support the test rotor. One slave TB rigidly attaches to the rig casing while the test TB connects to a load shaft supported on aerostatic bearings. The TBs, each with  $ID = 40.6$  mm and  $OD = 76.2$  mm, have eight pockets,  $20^\circ$  in arc length and 8.1 mm in radial length, with depth and feed orifice diameter equal to 0.51 mm and 1.80 mm for the test TB, and 0.44 mm and 1.55 mm for the slave TB, respectively. During operation, while the rotor spins to a maximum speed of 6 krpm (TB OD surface speed = 24 m/s), cold water at a maximum

supply pressure ( $P_s$ ) of 4.83 bar(g) lubricates the TBs. A calibrated taut string mechanism applies a static load ( $W$ ) on the movable shaft and which pushes the test TB against one end of the rotor collar. The rotor in turns transmits the same static load onto the slave TB. For dynamic load tests, a calibrated gun delivers impacts onto the load shaft and which excites both TBs and the rotor. The measurements include rotor axial displacements, load shaft acceleration, and the applied loads, static and dynamic. From these measurements, a mechanical system model aids to estimate the TB force coefficients; namely, stiffness ( $K_z$ ), damping ( $C_z$ ), and added mass ( $M_z$ ). For tests with a constant axial load ( $W$ ), the axial clearance ( $C_o$ ) increases as the TB lubricant supply pressure ( $P_s$ ) increases. Under a constant water supply pressure ( $P_s$ ) into the bearings, the test TB clearance ( $C_o$ ) decreases as the applied specific axial load ( $W$ ) increases to a maximum of 1.6 bar. The measured static load performance, agreeing with predictions as well as with earlier test results, demonstrates the TBs operate mainly as hydrostatic ones since hydrodynamic features derived from surface speed are small. From the multiple impact tests, for the TBs operating with a fixed supply pressure, the test TB experimental stiffness ( $K_z$ ) and damping ( $C_z$ ) increase as  $W$  increases, meanwhile the added mass ( $M_z$ ) varies slightly. Operation with a constant  $W$  and with an increase in water  $P_s$  yields an increase in  $K_z$  and  $C_z$  without a change of its added mass. Predictions agree well with the experimentally derived force coefficients. The test results are relevant to the pump industry, in particular for vertical lift processes.

## INTRODUCTION

In cryogenic fluid turbo pump applications, fluid film hybrid bearings offer an alternative to ultra-precision ceramic ball bearings for rotor support [1]. High shaft speeds typical of turbo pumps require the use of bearings with little or no surface speed limitation, a feature unique to fluid film (hydrostatic/hydrodynamic) hybrid bearings. These bearings allow a turbo pump to be smaller and lighter while operating with an increased mechanical efficiency.

San Andrés et al. (2016) [2] examine the performance of a test hydrostatic thrust bearing under an increasing static load (max. 3,600 N), shaft speed up to 17.5 krpm (tip surface speed = 70 m/s) and increasing supply pressure (max. 17.2 bar). The paper sums the work conducted by Forsberg (2008) [3], Ramirez (2008) [4], and Esser (2010) [5] in a research program designed to validate the technology of hybrid thrust bearings for application to cryogenic liquid turbo pumps. Measured parameters include flow rates (supply and return through thrust bearing inner diameter), pocket pressure, and fluid film clearance. In Refs. [2-5], predictions generated from a bulk flow model described in Refs. [6-7], accounting for fluid inertia and turbulent flow effects, agree well with the experimental results. As the applied load increases, predictions and measurements show that the film clearance and flow rate decrease exponentially. Measurements validate a predicted fluid starvation event at the highest speed and lowest supply pressure condition. Importantly enough, the measured flow rate and bearing pocket pressure enable the estimation of an empirical feed orifice discharge coefficient used to obtain accurate predictions.

Recently, in a program addressing to the needs of the subsea pumping industry, Rohmer et al. (2018) [8] report measurements of the static load performance of an eight pocket hybrid thrust bearing (HTB) lubricated with water at room temperature (24 °C), supply pressure to 4.14 bar (g), and operating with shaft speed to 3 krpm (12 m/s max surface speed). Under a constant applied load, the bearing axial clearance increases as the water supply pressure into the bearings increases. At a constant water supply pressure, and under an increasing axial load, the bearing axial clearance decreases to produce a reduction in flow rate and a higher pocket recess pressure. The test bearing static axial stiffness is derived based on the change in axial clearance as the applied static changes. The experimental results from the static load tests qualitatively match with predictions based on the analyses in Refs. [6-7]. Persistent angular misalignment between the test HTB and the rotor thrust collar caused a large uncertainty in the clearance measurements. Although the misalignment is quantified, it could not be eradicated without extensive modifications to the test rig.

Presently, the test rig in Ref. [8] is modified to conduct dynamic load tests on a water lubricated HTB and to identify the test bearing axial force coefficients; namely stiffness, damping and added or virtual mass. Note that the archival literature offers very few instances of experimentally derived damping coefficients and none for the added mass coefficient in a hybrid thrust bearing. A comparison of the experimentally derived HTB force coefficients against predictions serves to validate a predictive model; and hence, their engineered application in rotating machinery.

## DESCRIPTION OF TEST RIG AND THRUST BEARING

Figure 1 shows a photograph and cross section view of the thrust bearing test rig constructed to quantify the static and dynamic load performance of water lubricated hybrid (hydrodynamic/hydrostatic) thrust bearings (TBs). The rig consists of a single piece rotor supported on radial bearings, a drive motor and flexible coupling, and an axial load mechanism. The stainless steel rotor weighing 3.95 kg (8.7 lb) comprises of a long shaft and two end thrust collars. Two flexure-pivot, tilting-pad hydrostatic journal bearings, water lubricated, support the rotor weight. The radial bearings, made of 660 Bearing Bronze, are split into top and bottom halves to simplify the installation process. Both bearings have inner diameter and length equal to 38.1 mm and assembled with a radial clearance of 89  $\mu$ m. Each bearing has four pads, 72° arc extent, 60% pivot offset and null preload [2]. One rotor end is threaded for connection to a long quill shaft and diaphragm coupling attached to a variable frequency drive (VFD) motor, 25 kW and 25 krpm maximum rotational speed.

Two water-lubricated hybrid thrust bearings (HTBs), test and slave, see Figure 2, control the axial position of the rotor. The HTBs, manufactured with 660 Bearing Bronze, have inner and outer diameters equal to ID=40.6 mm and OD=76.2 mm, respectively. Each bearing has eight pockets, 20° in arc length, 8.13 mm in radial length, and with depth equaling 0.51 mm (test TB) and 0.44 mm (slave TB).

A loading mechanism pushes axially the test HTB to apply a load to the rotor thrust collar. As shown on the left of Figure 1, two

aerostatic radial bearings support the non-rotating shaft and allow its axial displacement with minimal friction when a load is applied. The rotor then transmits the load to the slave HTB.

Figure 3 shows a schematic view of the test rig with the thrust bearings and journal bearings represented as mechanical elements with stiffness and damping characteristics (radial and axial) [2]. Later, the assembly is represented as a one degree of freedom mechanical system for experimental identification of the test TB axial force coefficients (stiffness, damping, and added mass).

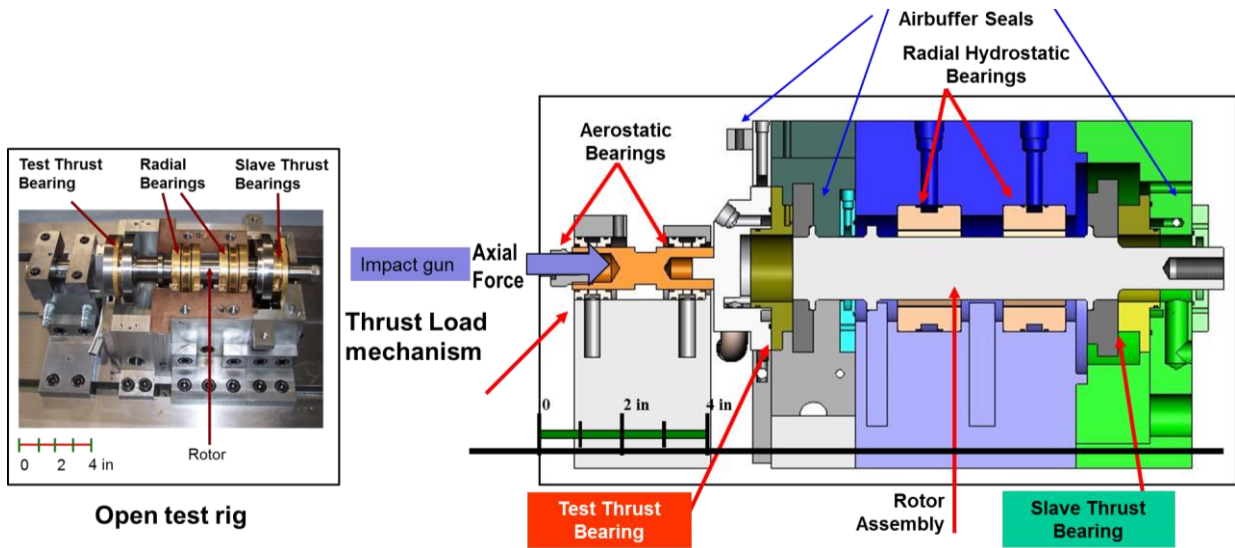
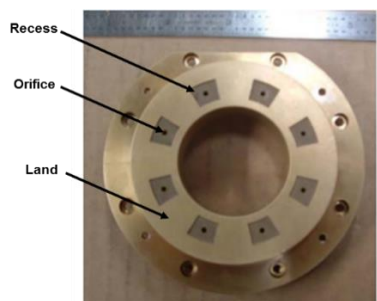


Figure 1. Photograph and cross sectional view of thrust bearing test rig [2].



Material	660 Bearing Bronze	Slave Bearing	Test Bearing
Thrust Face	Inner Diameter, $ID$	40.6 mm	
	Outer Diameter, $OD$	76.2 mm	
	Thrust Bearing Area, $A$	32.65 cm <sup>2</sup>	
Pocket	Number of Pockets	8	
	Arc Length	20°	
	Radial Length	8.13 mm	
	Depth	0.44 mm	0.51 mm
	Pocket/Wetted Area Ratio	0.19	
Orifice diameter, $d_{orif}$	1.80 mm	1.55 mm	

At 25 °C, water density  $\rho=995 \text{ kg/m}^3$  and viscosity  $\mu=0.89 \text{ cPoise}$

Figure 2. Photograph and physical parameters of test hybrid thrust bearing and water properties.

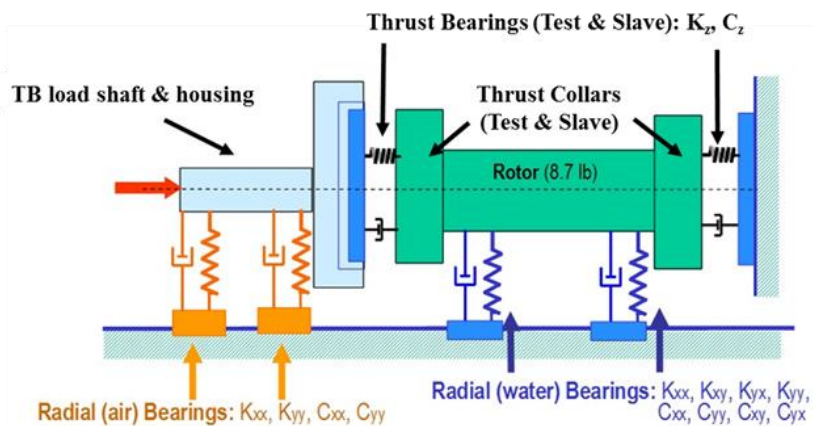


Figure 3. Schematic view of test rig with thrust and journal bearings represented as mechanical elements with stiffness and damping coefficients.

Figure 4 shows a schematic of the water supply system for the thrust bearing test rig which consists of a reservoir tank, main pump, return pump, heat exchanger, and various valves and instrumentation components [9]. A vertical 17 stage centrifugal pump and a 7 HP electric motor make up the main pump system operating at constant speed (1,450 rpm). Deionized water is supplied to the pump directly from a 500-gallon reservoir tank while flow to the test rig is controlled by a downstream globe valve that directs a portion of the flow back to the tank. A 2 HP, self-priming centrifugal pump routes the fluid exiting the test rig through an air-cooled heat exchanger and its return to the storage tank. Deionized water is beneficial for water-lubricated systems as it mitigates the effects of corrosion on the bearing metal surfaces and various system components decreasing down time and cost associated with cleaning and replacing components.

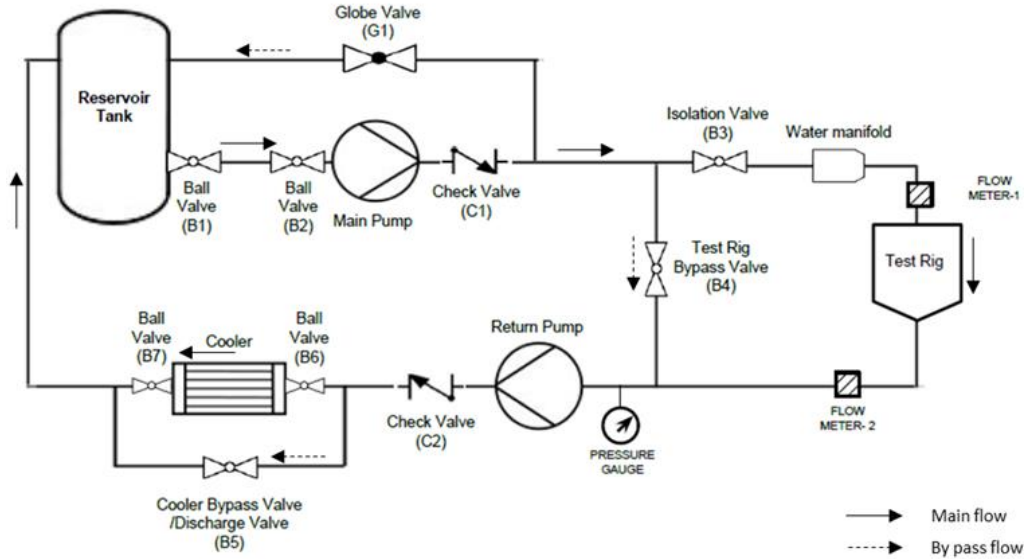


Figure 4. Schematic view of closed loop water supply system for thrust bearing test rig.

Prior research with the test rig involved only applying static loads to the test HTBs. For several years, many difficulties arose when attempting to apply simultaneously both static and dynamics loads as the test rig could not easily accommodate a shaker head. In the end, due to cost and time constraints, a system to excite the test bearing using impact loads was built. Note that although short time duration loads can excite a broad frequency range, their magnitudes are relatively small and do not produce significant shaft collar displacements. Hence, impact load testing demands of numerous individual tests and a subsequent averaging to reduce the amount of noise/signal interference [10].

Figure 5 depicts a diagram and a photograph of the ad-hoc mechanism built to apply both static and dynamic loads onto the test HTB. A taut steel cable slanted  $60^\circ$  relative to the load shaft applies a static load ( $W$ ) onto the test HTB. One end of the cable connects to a strain gauge load cell while the other end is affixed to the test rig base. The middle point of the taut cable crosses through a hollow tip which is fastened rigidly to a dynamic load cell (under compression) attached to the free end of the load shaft. Adjusting the cable tension ( $T_o$ ) sets the static load ( $W = 2 T_o \cos(60^\circ) = T_o$ ). The braided steel cable, 1.5 mm in diameter, when taut has a stiffness equal to  $K_C = 93.15 \pm 0.3 \text{ kN/m}$ ; see Wilkinson's thesis [11] for details. A horizontally placed impact load gun or hammer applies a short duration load onto the tip of the assembly to displace dynamically the load shaft and HTB.

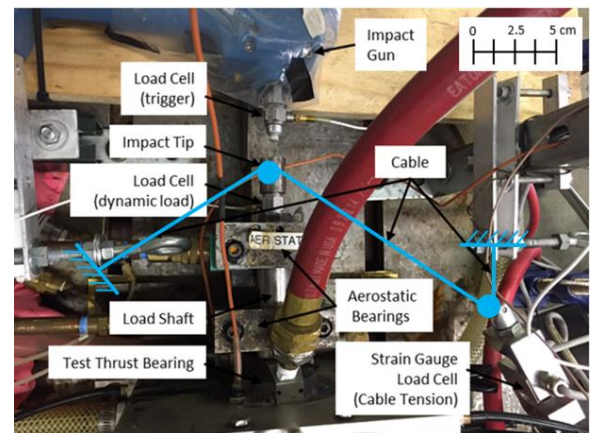
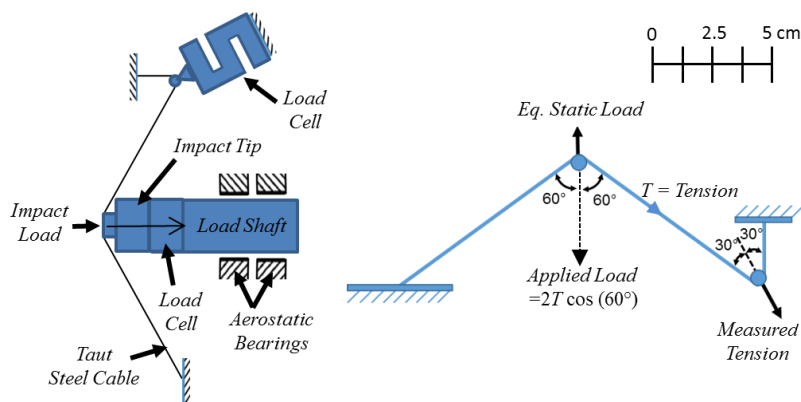


Figure 5. Schematic view, geometry and photograph of taut steel cable for static load application.

## TEST SYSTEM PHYSICAL MODEL AND PARAMETER IDENTIFICATION

Thrust bearing force coefficients, namely stiffness ( $K_z$ ), damping ( $C_z$ ) and added mass ( $M_z$ ), enable the prediction and control of axial rotor motions under dynamic loading. Obtaining reliable estimates of the bearing operating performance in actual test conditions is (although challenging) necessary to validate predictive models [12].

Figure 6 shows a schematic view of the test HTB and load shaft modeled as a one degree of freedom (1-DOF) system<sup>1</sup> with force coefficients ( $K_z$ ,  $C_z$  and  $M_z$ ). In the graph,  $z_{TTB}$  and  $z_R$  are the absolute axial displacements of the test TB and rotor, respectively, and  $z=(z_{TTB}-z_R)$  is the relative displacement between both components. The taut cable, whose stiffness is  $K_C$ , applies a static load ( $W$ ) to the load shaft, while simultaneously, an impact gun delivers a transient load  $F_d$ .

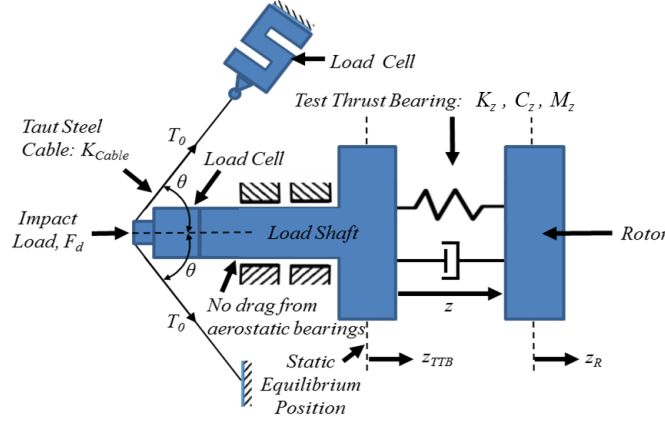


Figure 6. Schematic view of physical model for test HTB.

The instrumentation used includes six eddy current sensors (three on each HTB), one piezoelectric accelerometer affixed to the test HTB cartridge, and one load cell mounted on one end of the static loader. Measurements from the three displacement sensors define a plane and enable determination of the operating clearance at the center ( $C_o$ ) of both the test TB and slave TB, as well as the tilt angles, if any. See Ref. [2] for a complete description of the procedure to estimate  $C_o$ .

At a static condition, the equilibrium clearance  $C_o=z_o$  produces a test TB force  $W=T_o \cos(60^\circ)$ . Due to the impact load ( $F_d$ ), the test TB and rotor undergo small amplitude motions recorded by the displacement sensors, while an accelerometer measures the acceleration of the HTB and load shaft assembly.

Assuming no axial drag from the aerostatic bearings, the equation of motion (EOM) for the system undergoing axial motions is:

$$M \ddot{z}_{TTB} = W + F_{d(t)} - F_{TTB} - F_C \quad (1)$$

where  $M = 2.54 \text{ kg}$  is the mass of the assembly comprising the load shaft and test TB. The force exerted by the taut cable ( $F_C$ ) and the reaction force from the test bearing ( $F_{TTB}$ ) equal:

$$F_{C(t)} = W - K_C z_{TTB}, \quad F_{TTB} = F_{C_0} - [K_z z + C_z \dot{z} + M_z \ddot{z}] \quad (2)$$

The discrete Fourier transform operator (DFT) takes the force, displacement and acceleration data from the time domain into the frequency domain. Let

$$\bar{z}_{(\omega)} = DFT(z_{(t)}), \quad \bar{F}_{(\omega)} = DFT(F_{(t)}), \quad \bar{A}_{(\omega)} = DFT(\ddot{z}_{TTB(t)}) \quad (3)$$

where  $\omega$  denotes an excitation frequency. Hence, the EOM (1) in the frequency domain becomes

$$H_{(\omega)} = \bar{F}_{d(\omega)} + (K_C/\omega^2 - M) \bar{A}_{(\omega)} \rightarrow [K_z - M_z \omega^2 + i \omega C_z] \bar{z} \quad (4)$$

where  $H_{(\omega)}$  is the complex dynamic stiffness for the test element. The test TB axial force coefficients follow from curve fitting of the real and imaginary parts of

$$Re(H_{(\omega)}) \rightarrow (K_z - M_z \omega^2), \quad Im(H_{(\omega)}) \rightarrow C_z \omega \quad (5)$$

<sup>1</sup> The model assumes the face of the rotor thrust collar and TTB are parallel to each other. That is, there are no tilts. In practice this condition is rarely, if ever, achieved.

## STATIC LOAD PERFORMANCE OF TEST THRUST BEARING

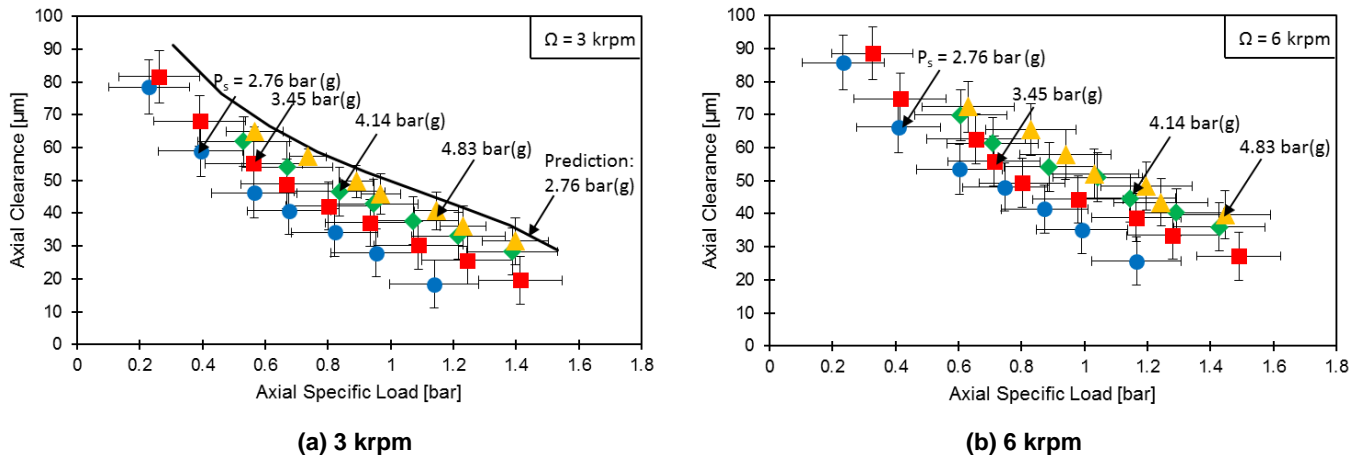
A series of experiments quantify the static load performance of the test HTB via measurements of the bearing axial clearance ( $C_o$ ) when operating under an applied axial load ( $W$ ) and with rotor speeds up to 6 krpm ( $\frac{1}{2} \Omega OD=24$  m/s). Meanwhile the thrust bearings, test and slave, are supplied with water at a set pressure ( $P_s$ ). During all tests water at a pressure of 3.45 bar(g) lubricates the radial bearings. The inlet temperature of the supplied water is ambient ( $\sim 24^\circ\text{C}$ ).

A test begins with a stationary rotor (not spinning) and as water supplies the axial test TB and slave TB with an increasing inlet pressure. A static load is then applied to the state TB using the cable tension loading system thus causing the bearing to load the thrust collar side of the rotor. The specific static load, i.e., load per unit area ( $W/A$ ) is used as a metric. Note  $A = 32.65 \text{ cm}^2 = \frac{1}{4} \pi (OD^2 - ID^2)$ . The slave TB reacts to the applied load transmitted by the shaft, thereby controlling the rotor axial position that sets the operating clearances of both thrust bearings. Finally, the electric motor gradually spins the rotor-coupling system up to the desired set speed.

A strain gauge pressure transducer, positioned just upstream of the test TB, records  $P_s$  that ranges from 2.76 bar(g) to 4.83 bar(g). With  $P_s$  held constant, the static load system pushes with a high load on the TTB and rotor to close any clearance. Immediately after, the load is reduced to generate the smallest clearance that enables the rotor to spin freely at the onset of testing. This operation avoids the risk of contact between the rotor collars and both thrust bearings for subsequent (lower) load conditions. If the rotor does not spin freely, the load shaft and TTB assembly must be realigned to the face of the thrust collar in the rotor. With a minimum (water lubricated) clearance established, the rotor is spun to a desired angular speed and a measurement conducted.

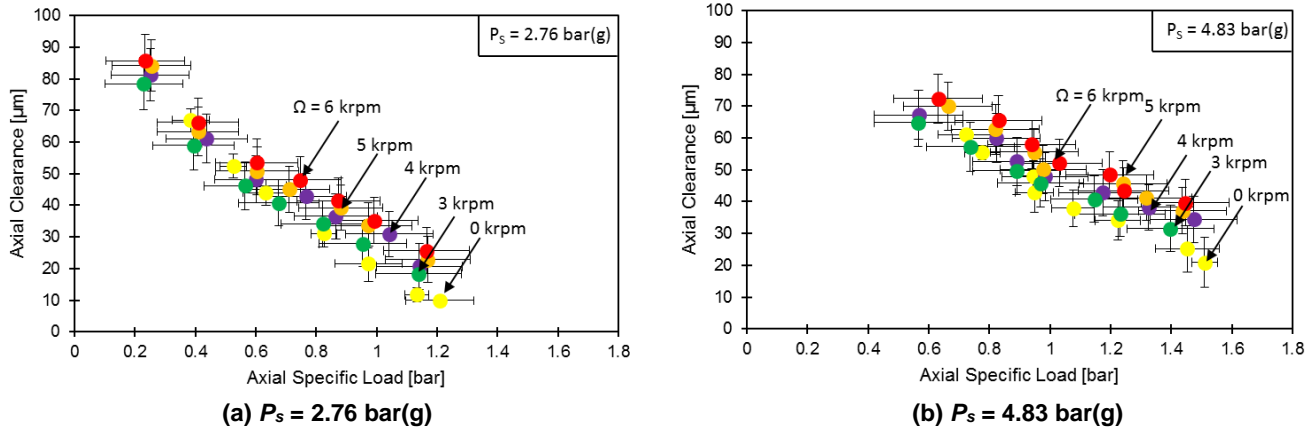
During a test, the axial clearance ( $C_o$ ) at the center of the test TB is derived from axial displacements obtained from three eddy current proximity sensors installed on the test TB housing at distinct angular locations, see Ref. [2]. The test rotor and bearings are not always perfectly aligned while the runout on the thrust collar is significant,  $\pm 10 \mu\text{m}$ . Hence, the acquired test data has a significant uncertainty [13]. A prior publication, Ref. [8], addresses with detail the persistent issue. Lastly, after the conclusion of a test conducted with a fixed shaft speed and varying the static load, the motor stops; and the process repeats with the bearings lubricated with water at a new set supply pressure.

Figure 7 depicts the measured test TB axial clearance ( $C_o$ ) vs. applied specific load ( $W/A$ ) for operation at two shaft speeds, 3 krpm and 6 krpm. Error bars, horizontal and vertical, denote the uncertainty of the measured applied load and clearance. Note that  $C_o$  decreases as the load increases though increasing with the operating shaft speed ( $\Omega$ ). More importantly,  $C_o$  raises as the water supply increases though the demand for flow raises. The figure includes a solid line representing a sample prediction, using the model in Ref. [6], for the test condition with  $P_s=2.76$  bar(g) and 3 krpm shaft speed. Predictions match qualitatively with the measurements although being consistently higher than the corresponding test data, i.e. average percent differences range from 25% to 53%. Earlier works [2, 9] report a better correlation between measurements and predictions.



**Figure 7. Measured TB axial clearance ( $C_o$ ) vs. applied specific load ( $W/A$ ) at two shaft speeds: 3 krpm and 6 krpm. Thrust bearings supplied with water at various supply pressures ( $P_s$ )= 2.76 bar(g) to 4.83 bar(g).**

To quantify the effect of shaft speed, 0 rpm to 6 krpm ( $\frac{1}{2} \Omega OD=24$  m/s), on the test TB static load performance, Figure 8 displays the measured TB axial clearance ( $C_o$ ) vs. specific load ( $W/A$ ) for operation with the bearings supplied with water at two pressures, 2.76 bar(g) and 4.83 bar(g) [40 psig and 75 psig]. At a constant TB supply pressure ( $P_s$ ) and as the shaft speed increases from 0 krpm to 6 krpm, the axial clearance increases slightly,  $\sim 10 \mu\text{m}$  for  $W/A=.4$  bar to  $\sim 20 \mu\text{m}$  at the largest load of or  $W/A=.4$  bar. The test data indicates that the hydrodynamic component of the bearing reaction force increases with both shaft speed and applied load. The null rotor speed condition represents a pure hydrostatic operation.



**Figure 8. Measured TB axial clearance ( $C_0$ ) vs. applied specific load ( $W/A$ ) at increasing shaft speeds. Thrust bearings supplied with water at two supply pressures ( $P_s$ ) = 2.76 bar(g) and 4.83 bar(g).**

## DYNAMIC LOAD PERFORMANCE OF TEST THRUST BEARING

### Force coefficients for test thrust bearing operating at 3 krpm and with an increasing water supply pressure

Prior to turning on the motor, 3.45 bar(g) pressurized water flows into the radial bearings allowing the rotor to spin freely by hand. Water then flows into the two thrust bearings, test and slave, with a constant pressure,  $P_s = 2.76, 3.45$  and 4.13 bar(g). The cable tension loading system, shown in Figure 5, applies static load ( $W$ ) on the load shaft and test TB. The same load acts on the rotor and the slave TB reacts to the applied load.

Next, the VFD motor gradually accelerates the rotor up to a set speed, ranging from 3 krpm to 6 krpm ( $\frac{1}{2} \Omega OD=24$  m/s). Upon meeting the test condition, a series of no less than 100 impact loads excite the load shaft and test TB along the axial direction ( $z$ ). The transient time response data (forces, displacements and accelerations) are collected at 31.25 k samples/s during  $\frac{1}{2}$  s, a total of 16,386 samples. Impact data sets are individually converted into the frequency domain and then averaged following the process in Ref. [10].

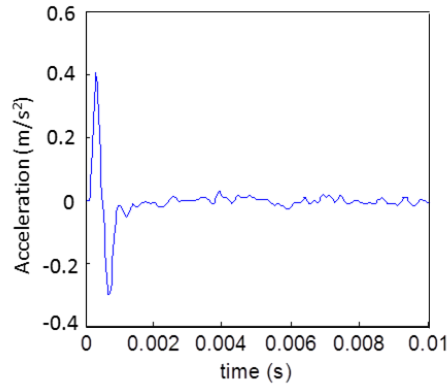
The analysis of the data in the frequency domain delivers the TTB complex dynamic stiffness,  $H(\omega)$ . Figure 9 shows an example of an acceleration time response due to an impact, as well as the real part of  $H(\omega)$  vs frequency<sup>2</sup> ( $\omega^2$ ) and the imaginary component of  $H(\omega)$  vs.  $\omega^2$ . The test TB damping coefficient  $C_z$  follows from a curve fit of  $\text{Im}(H) \rightarrow \omega C_z$ , whereas the bearing axial stiffness ( $K_z$ ) and added mass coefficient ( $M_z$ ) arise from the fit  $\text{Re}(H) \rightarrow (K_z - \omega^2 M_z)$ , as shown in Eq. (5).

Figure 10 shows the identified TTB force coefficients, namely stiffness, damping and added mass vs. water supply pressure ( $P_s$ ) into the TB and for operation at a shaft speed = 3 krpm ( $\frac{1}{2} \Omega OD=12$  m/s) and under three specific loads  $W/A = 0.55, 0.68$ , and 0.82 bar. Error bars evidence a large uncertainty, most due in part to the large run out of the thrust collar ( $\pm 10 \mu\text{m}$ ). Note repeatability or variability associated with the load impact test is rather low. Predictions are derived from the bulk flow model analysis in Refs. [6-7].

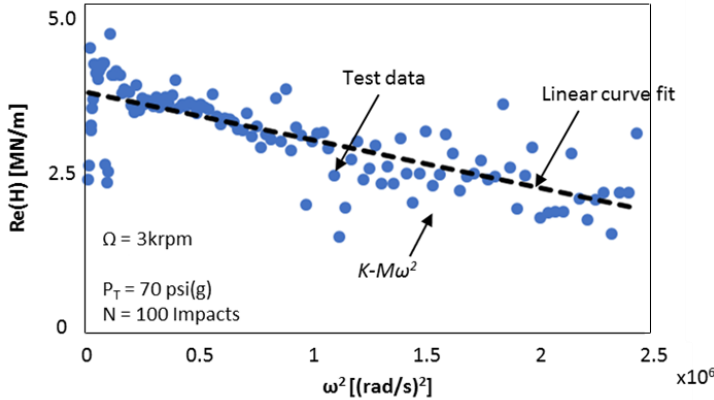
The axial stiffness ( $K_z$ ) increases with an increase in supply pressure. This behavior correlates well with the predicted stiffness although the rate of increase is higher than that of the experimental magnitude. A change in applied axial load has minimal influence on  $K_z$ , thus indicating  $P_s$  is the primary driver of stiffness for the test hybrid TB.

Both experimental and predicted damping coefficients ( $C_z$ ) increase with an increase in water supply pressure and are relatively insensitive to the applied load. The qualitative increase in experimental  $C_z$  agrees with predictions although the magnitude of the measured damping exceeds predictions for all but a test condition with  $P_s = 3.45$  bar(g) and  $W/A = 0.68$  bar. Similar to the stiffness, TB supply pressure  $P_s$  influences  $C_z$  more than applied load does.

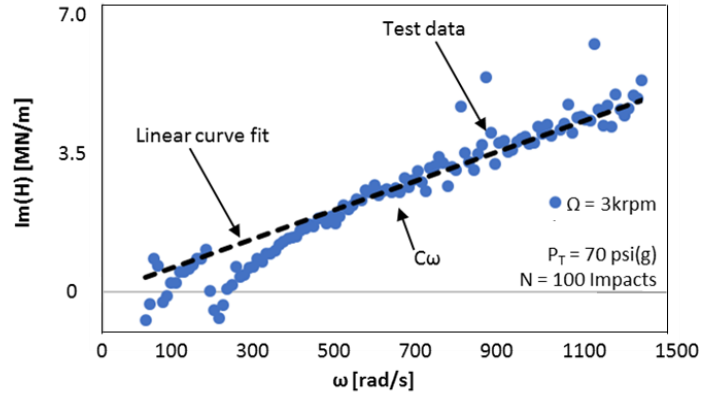
The experimentally identified TB added mass coefficient ( $M_z$ ) exceeds the predicted magnitude for all cases; the difference ranges from 8% to 32%. Both predictions and measurements show a minimal change in coefficient magnitude with an increase in water supply pressure into the TB. The maximum percent difference in  $M_z$  is  $\sim 29\%$  for  $W/A = 0.82$  bar as  $P_s$  increases from lowest to highest magnitudes. A simple estimate for  $M_z = [2 \rho A (OD+ID)] = 0.76$  kg, which is independent of the operating clearance  $C_0$  and agrees well with the predictions.



(a) Typical acceleration response of test TB due to an impact load



(b)  $Re(H)$  vs.  $\omega^2$



(c)  $Im(H)$  vs.  $\omega^2$

Figure 9. Typical TTB acceleration transient response and sample of average TTB complex dynamic stiffness, ( $H$ ) vs frequency ( $\omega$ ). Real and imaginary components of  $H$  and curve fits.

#### Force coefficients for test thrust bearing operating at increasing shaft speeds and with a constant water supply pressure

In another set of measurements, the TBs are supplied with constant pressure  $P_S=4.83(g)$  while the shaft speed increases from 3 krpm to 6 krpm, and as the applied load equals  $W/A = 0.55, 0.68$  and  $0.82$  bar. Figure 11 depicts the force coefficients ( $K_z, C_z, M_z$ ), experimental and predicted, vs. shaft speed. As  $W$  increases, the bearing stiffness  $K_z$  also increases while rotor speed has no effect on the coefficient magnitude. Predictions agree well with the experimental  $K_z$  and show the test TB performs primarily as a hydrostatic bearing.

Both predictions and experimental results reveal a minimal change in damping ( $C_z$ ) with an increase in rotor speed; however,  $C_z$  increases as the static load increases. Although the test damping magnitude exceeds the predicted one for  $W/A = 0.82$  bar, the magnitudes of predictions and measurements agree well overall. Lastly, predictions show no significant change in added mass ( $M_z$ ) with a change in shaft speed or applied load. The test results qualitatively agree with the prediction that rotor speed affects minimally  $M_z$ . However, the magnitude of the test results exceeds the predictions and evidence a raise in  $M_z$  with an increase in applied static load.

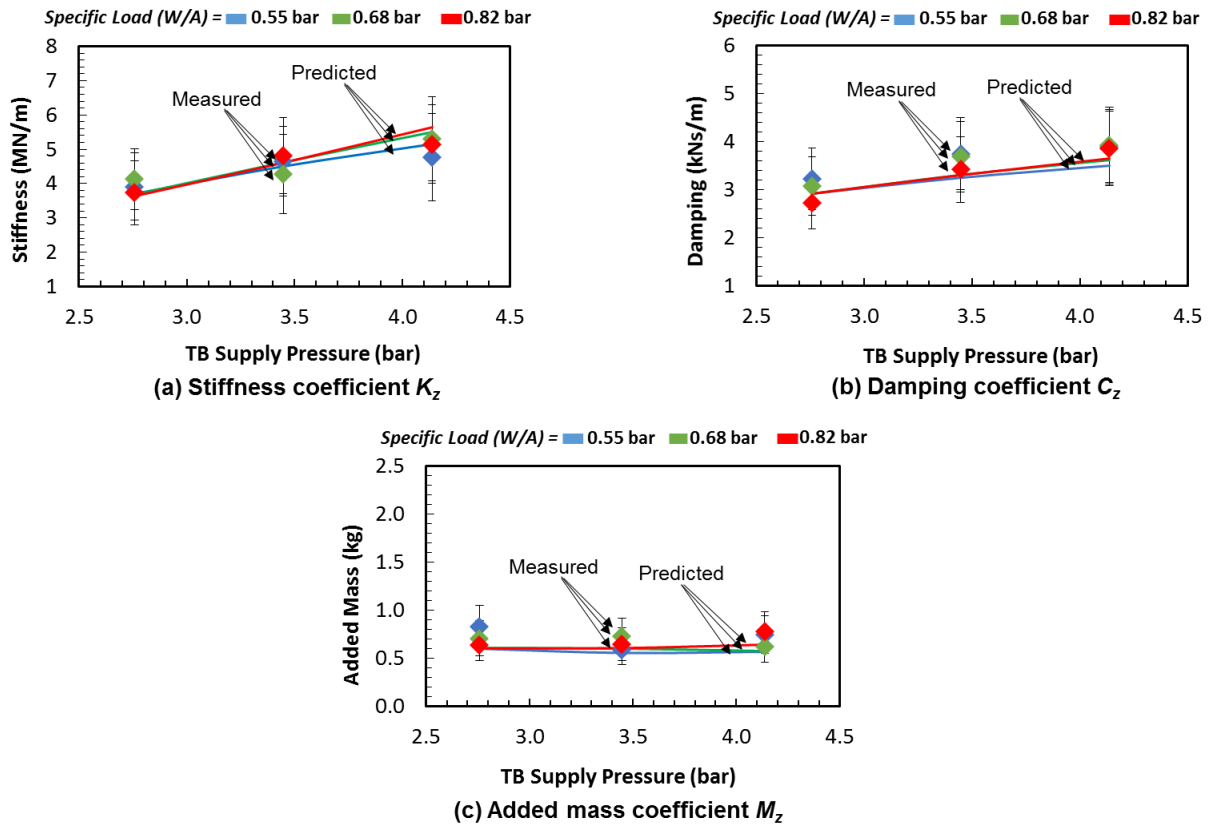


Figure 10. Experimental and predicted test TB force coefficients ( $K_z$ ,  $C_z$ ,  $M_z$ ) vs. water supply pressure. Operation at shaft speed =3 krpm and under three axial loads  $W/A = 0.55$  bar,  $0.68$  bar, and  $0.82$  bar.

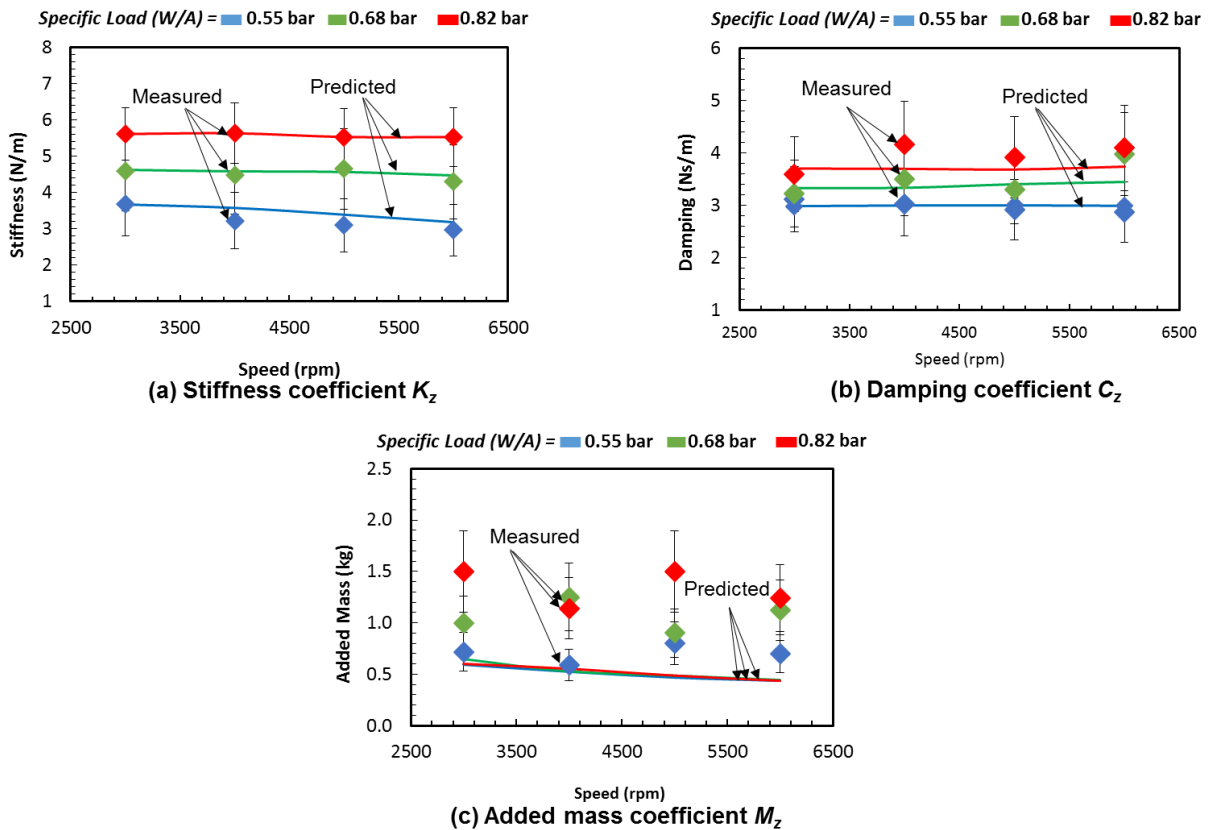


Fig 11. Experimental and predicted test TB force coefficients ( $K_z$ ,  $C_z$ ,  $M_z$ ) vs. shaft speed and three axial loads  $W/A = 0.55$  bar,  $0.68$  bar, and  $0.82$ . Water supply pressure  $P_s = 4.83$  bar(g).

## CONCLUSION

The technical brief presented a description of an ad-hoc test rig used for the evaluation of water lubricated hybrid bearings, thrust and radial, and produced experimental results for the axial film clearance of a hybrid thrust bearing operating at both increasing shaft speeds and static loads. Seldom reported in practice, the experiments also presents the test bearing axial force coefficients, in particular an added mass or virtual mass coefficient.

The measured static load behavior matches well with predictions as well as with prior experimental results. At a constant axial load, the axial clearance ( $C_o$ ) increases as the lubricant supply pressure ( $P_s$ ) into the TBs increases. With a constant  $P_s$ , however, the test TB axial clearance ( $C_o$ ) decreases as the applied axial load ( $W/A$ ) increases. Large uncertainties, inherent to the test rig construction and during operation, continue to plague the accurate measurement of the bearing axial displacement.

For operation with shaft speeds to 6 krpm ( $\frac{1}{2} \Omega$   $OD=24$  m/s), the dynamic forced performance of the test TB is measured through multiple impact load tests and force coefficients are derived from the system complex dynamic stiffness function. Measurements indicate that the test TB shows no appreciable change in dynamic force coefficients (axial stiffness, damping and inertia) with a change in rotor speed; hence the bearing behaves in a mainly hydrostatic mode as it lacks hydrodynamic features on the bearing surface such as tapered sections or tilting pads. With an increase in applied static load, however, the test TB stiffness and damping coefficients increase while the added mass coefficient remains relatively constant. For tests with an increasing static load, the experimental force coefficients agree well with predictions. Finally, with a constant applied load and at a low rotor speed (3krpm), an increase in TB supply pressure raises the axial stiffness and damping coefficients but the added mass does not change.

## NOMENCLATURE

$A$	$\frac{1}{4} \pi (OD^2-ID^2)$ . Thrust bearing area [ $m^2$ ]
$C_o$	Axial clearance between thrust bearing center and thrust collar [ $\mu m$ ]
$C_z$	Thrust bearing damping coefficient [Ns/m]
$F_{Cable}$	Force exerted by taut cable [N]
$F_d$	Applied dynamic (impact) load [N]
$F_{TTB}$	Thrust bearing reaction force [N]
$H$	Dynamic (complex) stiffness of thrust bearing = $H_R + i H_I$
$i$	Imaginary unit, $i = \sqrt{-1}$
$K_C$	Stiffness of taut cable = 93.15 kN/m
$K_z$	Thrust bearing stiffness coefficient [N/m]
$M$	Mass of load shaft and thrust bearing =2.54 kg
$M_z$	Thrust bearing added mass coefficient [kg]
$OD, ID$	Bearing outer and inner diameters, 76.2 and 40.6 mm
$P_s$	Water supply pressure [bar(g)]
$T_o$	Tension in taut cable [N]
$W$	$2 T_o \cos(60^\circ) = T_o$ . Applied static load with taut string on load shaft and test thrust bearing[N]
$z$	Relative displacement between rotor and test thrust bearing [ $\mu m$ ]
$z_R$	Absolute axial displacement of rotor [ $\mu m$ ]
$z_{TTB}$	Absolute displacement of test thrust bearing [ $\mu m$ ]
$\Omega$	Rotor speed [rad/s]
$\omega$	Excitation frequency [rad/s]

## ACKNOWLEDGEMENT

The authors thank the financial support and interest from the Turbomachinery Research Consortium (TRC) and the TEES Turbomachinery Laboratory at Texas A&M University.

## REFERENCES

- [1] Nosaka, M. and Kato, T., 2013, Cryogenic Tribology in High-Speed Bearings and Shaft Seals of Rocket Turbopumps, Dr. Jürgen Gagner (Ed.), DOI: 10.5772/55733.
- [2] San Andrés, L., Childs, D., and Phillips, S., 2016, “A Water Lubricated Hybrid Thrust Bearing: Measurements and Predictions of Static Load Performance,” ASME J. Eng. Gas Turbines Power, 139(2), pp. 022506-022506-10.
- [3] Forsberg, M., 2008, “Comparison Between Predictions and Experimental Measurements for an Eight Pocket Annular Hydrostatic Thrust Bearing,” M.S. Thesis, Mechanical Engineering, Texas A&M University, College Station, TX.
- [4] Ramirez, F., 2008, “Comparison between Predictions and Measurements of Performance Characteristics for an Eight Pocket Hybrid

- (Combination Hydrostatic/Hydrodynamic) Thrust Bearing,” M.S. Thesis, Mechanical Engineering, Texas A&M University, College Station, TX.
- [5] Esser, P., 2010, “Measurements versus Predictions for a Hybrid (Hydrostatic plus Hydrodynamic) Thrust Bearing for a Range of Orifice Diameters,” M.S. Thesis, Mechanical Engineering, Texas A&M University, College Station, TX.
- [6] San Andrés, L., 2000, “Bulk-Flow Analysis of Hybrid Thrust Bearings for Process Fluid Applications,” ASME J. of Trib., 122(1), pp. 170-180.
- [7] San Andrés, L., 2002, “Effects of Misalignment on Turbulent Flow Hybrid Thrust Bearings,” ASME J. of Trib., 124(1), pp. 212-219.
- [8] Rohmer, M., San Andrés, L., and Wilkinson, S., 2018, “Static Load Performance of a Water-Lubricated Hydrostatic Bearing,” J. Eng. Gas Turbines Power, 140(6), pp. 062401-062401-10.
- [9] Rohmer, M., Wilkinson, S., Jani, H. and San Andrés, L., 2016, “Measurement of Static Load Performance in a Water Lubricated Hybrid Thrust Bearing,” Annual Progress Report to the Turbomachinery Research Consortium, TRC-B&C-03-16, Texas A&M University, College Station, TX, May.
- [10] Santiago, O., San Andrés, L., 2007, “Field Methods for Identification of Bearing Support Parameters- Part I: Identification from Transient Rotor Dynamic Response due to Impacts,” ASME J. Eng. Gas Turbines Power, 129, pp. 205-212.
- [11] Wilkinson, S., 2019, “Measurements of the Static and Dynamic Load Performance of a Water Lubricated Hybrid Thrust Bearing,” M.S. Thesis, Mechanical Engineering, Texas A&M University, College Station, TX.
- [12] Tiwari, R., Lees, A.W., Friswell, M.I., 2004, “Identification of Dynamic Bearing Parameters: A Review,” Shock Vib. Dig., 36, pp. 99
- [13] Coleman, H., and Steel, W., 1989, “Experimentation and Uncertainty Analysis for Engineers,” John Wiley and Sons, Inc., pp. 1-71.